NONUNIQUENESS AND INSTABILITY OF CLASSICAL FORMULATIONS
OF NONASSOCIATED PLASTICITY, I: CASE STUDY

Thomas Pučik, Rebecca M. Brannon and Jeffrey Burghardt

msp

NONUNIQUENESS AND INSTABILITY OF CLASSICAL FORMULATIONS OF NONASSOCIATED PLASTICITY, I: CASE STUDY

THOMAS PUČIK, REBECCA M. BRANNON AND JEFFREY BURGHARDT

A dynamic instability, which is relatively unexplored in the literature despite having been long ago previously asserted to exist for any conventional nonassociated plastic flow model, is illustrated by means of an example problem. This instability is related to a condition known as achronicity, in which the wave speed in plastic loading is greater than that in elastic unloading (making it absolutely not related to the well-studied phenomena of localization and flutter). The one-dimensional example problem initializes an elastic-plastic half-space to a initially quiescent uniform state of prestress that places it in an achronic condition if a nonassociated flow rule is used. The initial stress state is perturbed by an axial stress pulse applied at the surface. The problem is first solved analytically for the case of constant wave speeds, and it is shown to possess a two-parameter family of nonunique solutions. These solutions are unstable in that both the amplitude and the width of the propagating pulse increase linearly with time. The case-study problem technically represents spontaneous motion from a quiescent state, but it does not violate thermodynamics (as the energy driving the instability is available from elastic stored energy of the initial prestress). The example problem is additionally solved numerically for both constant and nonconstant plastic wave speeds, where the instability is observed in either case. Furthermore, it is shown that neither the constant nor the nonconstant wave speed solution converges with mesh refinement, which therefore represents a numerical inadmissibility associated with the underlying loss of uniqueness of solution. It is the nonuniqueness of the unstable solution, not the existence of the instability itself, that is of primary concern. Unlike conventional localization instability, this achronic instability is not yet known to be a real phenomenon. This case-study problem illustrates the need for novel laboratory testing methods sufficient to determine if the instability is truly physical, or merely an anomalous shortcoming of classical nonassociated plasticity formulations. Some guidance for appropriate laboratory testing is presented, with emphasis on why such testing is highly nontrivial as a result of irreducible uncertainty in direct validation of a regular flow rule.

1. Introduction

Plastic flow is said to be nonassociated if the plastic strain increments are not normal to the yield surface in stress space. This type of flow is of particular interest in applications involving geological materials, which often exhibit apparent nonassociated behavior in quasistatic laboratory tests. Nonassociated flow rules are also employed quite frequently in numerical simulations, because associated flow rules appear to significantly over-predict the amount of plastic dilatation for most materials [Spitzig et al. 1975; 1976; Lade et al. 1987; Shen et al. 2012], and because (by allowing a simple radial return for such materials) they are easier to implement than associated flow rules. In this century, it has been shown that a conventional associated flow rule also cannot describe the anisotropic behavior of rolled sheet metal [Stoughton 2002;

Keywords: plasticity, flow rule, nonassociated flow rule, instability, incremental nonlinearity.

Cvitanic et al. 2008; Mohr et al. 2010; Taherizadeh et al. 2010]. Gao et al. [2011] have shown that a nonassociated flow rule more accurately describes the behavior of aluminum under a variety of loading conditions, but their loading conditions did not include the type of loading that we explore in this paper. Somewhat more recent work [Desmorat and Marull 2011; Dunand et al. 2012; Besse and Mohr 2012] has shown that a nonassociated flow rule is not necessary to describe the anisotropic plasticity of rolled sheet metal if other plasticity features are included.

The models discussed above are macroscopic phenomenological models, which do not directly account for a material's complex microstructure. Rousselier et al. [2012] have shown that in the case of metals plasticity, microstructural based models, which have a more complex formulation not compatible with classical macroscale phenomenological plasticity frameworks, are better suited to describe the complex evolution of a material undergoing plastic flow. Alternatives to traditional plasticity models are discussed and examined in more detail in the companion (part II) paper.

An assertion that nonassociated flow may stimulate instability and/or nonuniqueness is certainly not new, but the particular case of so-called "achronicity" (in which plastic stiffness exceeds elastic stiffness) seems to have been relatively unexplored in comparison to unrelated phenomena such as localization or flutter associated with a zero, negative, or complex plastic acoustic eigenvalue. Early initial concerns about achronicity were motivated by the observation that with nonassociated flow, it is possible to find closed loading cycles for which useful energy could be extracted from the material and the system of forces acting on it. This was first pointed out by Drucker [1949; 1950] for closed stress cycles, and later by Il'Yushin [1961] for closed strain cycles. This is not a violation of conservation of energy, since the released energy is merely liberated from stored strain energy associated with the ambient initial prestress. The major concern was that this might lead to an unstable release of energy under some conditions. However, no specific (and generally applicable) mechanisms for causing such unstable energy releases to occur were identified in this early work. For a more detailed discussion of these and other concerns about insufficient substantiation of a nonassociated flow rule (which is not tantamount to ruling it out altogether), see Brannon [2007].

The first concrete example of an actual plastic instability was a strain localization instability first identified by Rudnicki and Rice [1975]. This particular form of instability was found to result from a softening-like behavior caused by nonassociated flow. Rudnicki and Rice showed that, with nonassociated flow, this type of instability can occur even for positive values of the hardening modulus under certain conditions. With associated flow, on the other hand, it was shown that it can occur only for negative values of the hardening modulus (i.e., by putting explicit strain softening into the material model).

Another form of instability related to nonassociated plastic flow is called the flutter instability, first identified by Bigoni [1995]. The strain localization instability and the flutter instability result from the fact that the elastic-plastic tangent stiffness tensor loses positive definiteness when the yield function and flow potential function are not coincident. Strain localization is a result of the occurrence of a negative acoustic eigenvalue, whereas the flutter instability corresponds to complex eigenvalues. The "achronic" state, discussed in this paper, corresponds to *positive* plastic acoustic eigenvalues — but with a plastic eigenvalue being larger than any of the elastic eigenvalues, hence implying plastic wave speeds exceeding elastic wave speeds. For a complete derivation of conditions for all possible magnitudes of plastic wave speeds relative to elastic speeds, see Brannon and Drugan [1993].

Sandler and Rubin [1987], as well as Sandler and Pučik [1993], investigated the fundamentally different form of instability that has been virtually ignored in comparison to now-ordinary localization or flutter. The mechanism underlying this instability is, in many respects, the diametrical opposite of the softening mechanism investigated by Rudnicki and Rice. That is, it is found that nonassociated flow can also lead to excessive *stiffening* under certain conditions. This can cause the incremental modulus (and hence the wave speed) of the material to be greater in plastic loading than it is in elastic unloading. Under these loading conditions the eigenvalues of the tangent operator remain real and positive.

Sandler and Rubin used a simple case-study problem to show that this wave speed inversion, which is referred to in this paper as *achronicity*, is a dynamically unstable condition in that, when it occurs, there always exist loading paths for which the solution to the equations of motion becomes unstable in the sense that both the amplitude and width of a finite stress wave, no matter how small, grows without bound as it propagates into material at yield. This phenomenon is essentially spontaneous motion from a quiescent state, but not necessarily a violation of thermodynamics, since energy to drive the instability could come from elastic prestress.

The question remains, however, whether or not it is possible to observe such behavior in the laboratory. This paper (or its companion, part II) encourages such efforts by describing the expected character of achronic material response and its sensitivity to details of the flow rule. Additionally, Sandler and Rubin demonstrated that, for their simple case-study problem, the governing equations admit multiple solutions and are thus ill posed, which has significant implications for numerical modeling. In this paper, any instability that arises from achronicity is referred to as the Sandler–Rubin instability.

Unlike the localization and flutter instabilities, the Sandler–Rubin instability has been shown to emerge only under a specific class of initial boundary-value problems where both the elastic unloading and the elastic-plastic loading branch of the constitutive operator are exercised. Therefore, this instability is fundamentally different from the other instabilities mentioned in that it does not arise directly from the plastic flow itself.

Stoughton and Yoon [2008] have asserted that Sandler and Rubin's analysis is invalid since their solutions "do not generally solve the dynamic equations of motion unless the components of the constitutive models are such that the slope of the stress-strain relation, the gradient of the plastic potential and the gradient of the yield function are constant for a finite perturbation." The (flawed) rationale for this assertion is that "if C_L [the wave speed in plastic loading] is not constant to first order in the time step, then it is easy to see that the solution [the Sandler–Rubin solution] does not solve the equations of motion for any finite time step $\Delta t > 0$." It is true that Sandler and Rubin's solution becomes invalid for the case of nonconstant wave speeds, but that is because the *solution itself is specifically for the case of constant wave speeds* (more correctly, the solution is for piecewise constant wave speeds, depending on the plastic state of the wave characteristic). Almost as a tautology, the solution of problem should never be expected to apply without revision to cases that violate the original solution's assumptions. Since the assumption of a constant wave speed (a consequence of assuming nonhardening plasticity and linear elasticity) was made in the derivation of Sandler and Rubin's analytical solutions, one would not expect those solutions to solve the equations of motion under other conditions. This would be akin to deriving an elasticity solution while assuming a constant elastic modulus, then attempting to substitute a nonconstant elastic modulus into the resulting solution. It would be an enormous coincidence if the resulting expression still satisfied the governing equations. The fact that Sandler and Rubin's constant-wave-speed solution

does not solve the equations of motion for nonconstant wave speeds does not rule out the possibility of a similar instability and nonuniqueness in the nonlinear case (which has no analytical solution, to our knowledge). The present paper seeks to substantiate this point through a counterexample by solving a problem similar to the one solved by Sandler and Rubin, but with the addition of nonlinear hardening, which results in nonconstant plastic wave speeds but does not eliminate the instability or its associated nonuniqueness.

To our knowledge, only two studies have attempted to investigate the existence of this instability experimentally. In the first of these, Lade et al. [1987] performed a set of quasistatic triaxial compression tests using sand to investigate any possible instabilities arising from a violation of Drucker's postulate. The study found that no instabilities were observed even for loading directions which produce a negative inner product of the stress rate and plastic strain rate tensors. However, instability was defined in that work as "gross collapse". The Sandler–Rubin instability discussed in this paper is actually the result of a stiffening of the material, which (if real) might manifest as unstable waves that grow so slowly in amplitude that they can be quenched from boundary release waves before inducing "gross collapse". Thus, Lade's observations neither confirm nor rule out a Sandler–Rubin instability.

More recently, Brannon et al. [2009] conducted an extensive suite of quasistatic triaxial compression measurements within the loading regime where Sandler and Rubin's analysis would predict instability. As with Lade's study, no evidence of instability was observed, but the data were not extensive enough to firmly rule out a Sandler–Rubin instability either. Whether or not the Sandler–Rubin instability is actually a nonphysical mathematical anomaly remains unclear, as it has eluded direct laboratory efforts to date.

At least within classical plasticity formulations that neglect elastic-plastic coupling and other sources of so-called phantom nonassociativity [Brannon 2007], it can be proved mathematically that having a plastic flow direction different from the direction of the yield surface normal implies existence of loading modes for which achronicity occurs [Sandler and Pučik 1993; Brannon and Drugan 1993], even for infinitesimal strain increments. This includes any nonassociated material obeying the Prandtl–Reuss flow rule, which is the basis for the "radial return" algorithms employed in many of the material models used in numerical simulations (primarily because it is very easy to implement). Accordingly, one would expect achronicity to be very common in numerical simulations. Yet, nonassociated flow rules have been used in numerical calculations for more than three decades, and in most cases it is difficult to identify any obvious ill effects in the numerical results. A number of factors may account for achronic instability being subtle enough to miss despite being present in a simulation:

(1) Achronic instabilities are fairly weak, with growth rates that are typically only linear with time. Unlike exponential runaways, for example, they don't usually call attention to themselves by crashing a code through excessive deformation leading to "gross collapse".

(2) At least in our case-study simulations, achronic instabilities don't leave easily recognized signatures, such as the shear bands one typically gets with strain localization instabilities. The residual effects are much more spread out, and easily masked in complex problems.

(3) Achronic instabilities always entail characteristic deformation modes, most of which are three-dimensional, and hence are artificially disallowed in two-dimensional calculations. This situation is analogous to a 1-D bar compression simulation being incapable of manifesting a buckling instability.
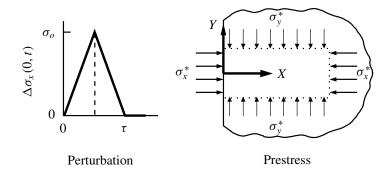
Figure 1. Geometry, loading, and coordinate system in the example problem.

(4) Nonuniqueness is very difficult to detect in numerical calculations. Even if many solutions are possible, a digital computer will always give one and only one answer. When nonuniqueness is associated with instability, nonconvergence and other forms of mesh sensitivity are typical symptoms of ill-posedness of governing equations.

Moreover, achronic instabilities weren't even known to exist until fairly recently. Most analysts have been (and still are) unfamiliar with their features, and may not be aware of what to look for, thus motivating this work. The purpose of part I of this paper is to illustrate some of these features by means of an example problem. Part II of this paper discusses possible ways that the instability may be influenced or eliminated altogether. The example problem is designed to be simple enough so that the effects of instability and nonuniqueness can easily be isolated, highlighted, and independently confirmed by any researcher with access to simple nonassociated plasticity codes (provided that the software allows a nonzero initial stress).

2. Problem description

In this section we present an example problem that exhibits achronicity. This problem is designed to be the simplest possible that exhibits achronicity. The primary reason for choosing such a simple problem is to allow an analytical solution to be derived. Examining achronicity via an analytical solution allows the nature of the instability and nonuniqueness to be made clear. Based solely on the simple example problem presented here it cannot be ruled out that the instability or nonuniqueness might be eliminated under a more complex model, but there is no reason to believe that the example presented here represents a special case. More complex models will be explored in part II. Despite its simplicity, the problem presented here is physically plausible and uses a model that is a member of a widely used class of traditional plasticity models. The parameters used in the problem are within typical ranges for geologic materials.

The example is a one-dimensional problem of an elastic/plastic half-space that is initially quiescent, but in a uniform state of prestress placing it in an achronic condition, which is subsequently perturbed by an axial stress pulse applied at the surface. The geometry, loading, and coordinate system are illustrated in Figure 1. The material properties and initial stress state, denoted by σ_{ij}^*, are chosen so that achronicity is satisfied with respect to longitudinal wave propagation in the x-direction.

The applied axial stress perturbation $\Delta\sigma_x(0, t)$ at the surface is a triangular pulse designed to produce plastic loading followed by elastic unloading.[1] Because the material is in an achronic state, the loading ramp travels faster than the unloading ramp as the pulse propagates to the right. This causes the two ramps to separate, which has two important consequences. First, the pulse width increases with time. Second, the region between the two ramps, which initially consists of just a single point (the apex of the triangle), opens up into a finite region. The solution in this region is indeterminate in that it is not dictated by either the initial or the boundary conditions, as is normally the case in well-posed initial/boundary value problems for hyperbolic equations. As a result, the solution in this region is unstable and nonunique.

In the following discussion, the example problem is analyzed both analytically and numerically. First, an analytical solution similar to Sandler and Rubin's is derived assuming perfect plasticity, which results in a constant plastic wave speed. For this case, it is shown that it is possible to derive a two-parameter family of nonunique solutions to this problem. These solutions are also shown to be unstable in that both the width and the amplitude of the pulse increase linearly with time. The constant-plastic-wave speed problem is then analyzed numerically using the finite-element method, and the results are shown to be consistent with the analytical solutions in the sense that the numerical solutions appear to belong to the infinite set of nonunique analytical solutions.

The problem is also solved numerically using a nonlinear hardening law, which results in a nonconstant plastic wave speed. For both the constant and nonconstant wave speed case, it is shown that the numerical solution does not converge as the mesh is refined, but that the numerical solution becomes more noticeably unstable with mesh refinement. Specifically, the instability magnitude grows even as the time step is reduced to values much lower than that required for ordinary Courant time integrator stability. This lack of convergence with mesh refinement is, we believe, the result of the ill-posedness of the underlying equations of motion. The link between ill-posed governing equations and nonconvergence of numerical solutions has been likewise well established for other — *but unrelated* — sources of ill-posedness such as localization (cf. [de Borst et al. 1993]).

We begin the discussion of the Sandler–Rubin case study by first completing the problem definition, and demonstrating that achronicity does indeed exist for the specified material properties and initial state.

2.1. *Material properties.* Except as discussed below, the material properties are based on representative values for limestone rock. The elastic properties are taken as

$$\rho = 2500\,\text{kg/m}^3,$$
$$E = 30\,\text{GPa},$$
$$\nu = 0.25,$$

where ρ is the mass density, E is Young's modulus, and ν is Poisson's ratio. For the *analytical* solution, only ideal linearized plasticity is assumed. Section 5 shows that *numerical* solutions, including both linear and nonlinear hardening, likewise exhibit the same general characteristics as the analytical solution

---

[1]The first leg of this axial stress pulse is tensile in the sense that it causes a reduction in the compressive stresses relative to their prestress values. Even though the first leg of this pulse reduces the stresses (in absolute value), it is referred to as "loading" because it induces plastic flow. The second leg, which increases the stress magnitude, is termed an unloading leg because it corresponds to elastic deformation driving the final stress state to a point inside the yield surface.

(namely, instability and nonconvergence, which is symptomatic of nonuniqueness/ill-posedness of the governing equations in the presence of achronicity).

To construct the simplest possible case study exhibiting achronistic instability, the yield surface is taken to be of Drucker–Prager form,

$$f(\boldsymbol{\sigma}) = \sqrt{J_2} + \alpha I_1 - k = 0, \tag{1}$$

where $I_1 = \mathrm{Tr}(\boldsymbol{\sigma})$ is the first invariant of the stress tensor, and $J_2 = \frac{1}{2}\boldsymbol{S} : \boldsymbol{S}$ is the second invariant of the deviatoric stress tensor $\boldsymbol{S}$. Stresses are taken to be positive in tension, so the preconfinement stresses (defined below) will be negative. The values for the constant material parameters, α and k, are in a typical range for limestone:

$$\alpha = 0.315,$$
$$k = 5.066\,\mathrm{MPa}.$$

These values correspond to a friction angle of 40° and a cohesion of 4.5 MPa.[2]

The flow rule, typical of what is adopted in engineering applications of phenomenological rock plasticity, is

$$\dot{\boldsymbol{\epsilon}}^p = \dot{\lambda}\widehat{\boldsymbol{M}}, \tag{2}$$

where $\dot{\lambda}$ is the magnitude of the plastic strain rate tensor, and $\widehat{\boldsymbol{M}}$ is a second-order unit tensor in the direction of the gradient of the plastic potential function

$$g(\boldsymbol{\sigma}) = \sqrt{J_2} + \alpha_p I_1. \tag{3}$$

If α_p is chosen to be equal to α, then the flow rule is said to be associated. The solutions hereafter presented are for the case when $\alpha_p = 0$, which corresponds to the Prandtl–Reuss flow rule.

2.2. *Initial and boundary conditions.* The region is initially quiescent but in a uniform state of prestress, $\boldsymbol{\sigma}^*$, which is a state of conventional triaxial compression in the x-direction. The values for the initial state are taken as

$$\sigma_x^* = -100.00\,\mathrm{MPa}, \tag{4}$$
$$\sigma_y^* = \sigma_z^* = -17.55\,\mathrm{MPa}, \tag{5}$$

and zero shear stress. Noting that these values are both negative, this initial stress is in a state of compression. For the assumed values of α and k, this state is on the yield surface defined by (1).

---

[2]The friction angle, ϕ, and cohesion, c, are related to the constants α and k. However, there is more than one definition that may be used. The one assumed in this discussion is based on a conventional triaxial compression loading condition, which results in the following expressions:
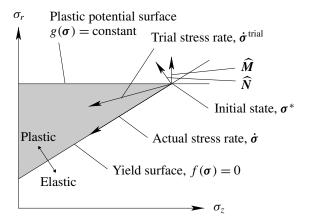
$$\alpha = \frac{2\sin\phi}{\sqrt{3}(3 - \sin\phi)} \quad \text{and} \quad k = \frac{6c\cos\phi}{\sqrt{3}(3 - \sin\phi)}.$$

Figure 2. Illustration of the initial state with the yield surface, defined by $f(\boldsymbol{\sigma}) = 0$, and plastic flow potential isosurface $g(\boldsymbol{\sigma})$ shown in the meridional profile defined by Lode stress invariants ($\sigma_r = \|\boldsymbol{S}\|$ and $\sigma_z = -\text{Tr}(\boldsymbol{\sigma})/\sqrt{3}$, which are similar to the q and p invariants commonly used in geomechanics, but scaled to make this plot isomorphic to stress space). $\widehat{\boldsymbol{M}}$ is the direction of the plastic strain rate, which is normal to the plastic flow potential isosurface. The vector labeled $\dot{\boldsymbol{\sigma}}^{\text{trial}}$ is defined to be the elastic stiffness acting on the total strain rate, which is the stress rate that would result if the material response were elastic under the same total strain rate. The vector labeled $\dot{\boldsymbol{\sigma}}$ is the actual stress rate, which remains on the yield surface.

The axial stress perturbation (applied at the surface of the half-space) is a triangular pulse characterized by a peak axial stress σ_o and a pulse duration τ, as illustrated in Figure 1. The values for these quantities are taken as

$$\sigma_o = 10\,\text{MPa} \tag{6}$$

and

$$\tau = 2\,\text{ms.} \tag{7}$$

Since σ_o is positive, this perturbation is actually tensile (i.e., it slightly reduces the initial precompression). Accordingly, the motion at the surface is initially outward (to the left) followed by a restoring motion that is inward (to the right).

2.3. *Loading in stress space.* The initial state and the elastic perturbation are illustrated in Figure 2, as viewed in the meridional (constant Lode angle) plane of the isomorphic stress invariants. The principal stresses σ_1, σ_2, and σ_3 correspond to the actual stresses σ_{xx}, σ_{yy}, and σ_{zz}, respectively.

The trial elastic stress rate $\dot{\boldsymbol{\sigma}}^{\text{trial}}$ is defined to be the elastic stiffness acting on the total strain rate tensor.[3] For a stress state at yield, a loading increment is plastic if and only if the trial elastic stress rate

---

[3]The trial elastic stress rate is not generally equivalent to the so-called "test" elastic stress rate that corresponds to a purely elastic solution consistent with boundary conditions. As pointed out by Brannon [2007], the two are equivalent only under conditions of prescribed strain (as is the case in constitutive models called by finite element codes, where traction boundary conditions are enforced as explicit contributions to the boundary integral of the weak form of the equations of motion, not as stress constraints in the constitutive model).

has a positive inner product with the normal to the yield surface. Figure 2 shows that plastic loading (for a nonassociative model like this one) does not require the trial elastic stress rate to have a positive inner product with the flow direction. In particular, our case study is specifically designed to be a uniaxial-strain wave-propagation problem for which the axial stress rate at the boundary generates a *trial* stress rate pointing into the shaded wedge in Figure 2, which is above the yield surface (hence plastic) but below the flow surface. The direction of trial elastic stress rate, cast as a vector in principal stress space, is determined from the fact that the deformation mode associated with the perturbation is a uniaxial strain increment in the x-direction, which implies the following relationship between the lateral and axial elastic increments:

$$\dot{\sigma}_2^{\text{trial}} = \dot{\sigma}_3^{\text{trial}} = \frac{\nu}{1-\nu}\dot{\sigma}_1^{\text{trial}}, \tag{8}$$

where ν is Poisson's ratio. This determines the direction of $\dot{\boldsymbol{\sigma}}^{\text{trial}}$ to within a sign. The sign is determined by demanding that $\dot{\boldsymbol{\sigma}}^{\text{trial}}$ be directed outward from the yield surface, so that the response is plastic rather than elastic. As seen in Figure 2, this requires $\dot{\sigma}_1^{\text{trial}}$ to be positive, which corresponds to a tensile axial stress increment. The magnitude of $\dot{\boldsymbol{\sigma}}^{\text{trial}}$ is set by requiring the axial stress perturbation $\dot{\sigma}_1^{\text{trial}}$ to equal 10 MPa (as selected in (6)).

By design, and as can be seen in Figure 2, the trial elastic stress perturbation falls within the shaded, wedge-shaped region above the yield surface but below the plastic potential surface. This type of loading causes work done on the material in a closed strain cycle to be negative—i.e., the material does net positive work on its surroundings [Sandler and Rubin 1987; Sandler and Pučik 1993]. As might be expected, there is a close relationship between negative work and achronicity. Unfortunately, this relationship is difficult to demonstrate in general due to the complexity of the deformation modes typically needed to induce it. These loading paths are generally difficult to attain in the laboratory as well [Brannon et al. 2009], and always involve nonproportional loading. However, for the special case of longitudinal wave propagation considered in the example problem, it can easily be seen. Because the deformation mode in this case is uniaxial strain in both loading and unloading, it is easily shown that the work ΔW done in a closed strain cycle $\pm\epsilon_1$ is given by

$$\Delta W = -\tfrac{1}{2}(M_L - M_U)(\Delta\epsilon_1)^2, \tag{9}$$

where M_L and M_U are the constrained moduli[4] in loading and unloading, respectively. Accordingly, it follows that $\Delta W < 0$ if and only if $M_L > M_U$. In other words, negative net work in this closed strain cycle will occur if the modulus (and hence the wave speed) in loading is greater than that in unloading. The values of the moduli and wave speeds are derived in the next section, and it is shown that this condition is, in fact, satisfied for the example problem.

From Figure 2, it is also apparent that, for the type of loading considered in this problem, plastic loading (i.e., a trial stress rate pointing above the yield surface) actually corresponds to physical unloading (i.e., a reduction in the magnitude of stress). The elastic unloading phase (which has a trial stress rate pointing below the yield surface) actually corresponds to physical loading (i.e., an increase in the magnitude of stress). In this paper (unless otherwise indicated), "loading" and "unloading" always refer to plastic loading and elastic unloading relative to the yield surface. As previously indicated, plastic loading for this case study occurs during a stress-releasing increment.

---

[4]i.e., slopes of the axial stress-strain plot in uniaxial strain conditions.

3. Proof of achronicity

This section demonstrates that the case study's initial state and specified boundary loading conditions induce an achronistic condition (where plastic stiffness exceeds elastic stiffness). The loading and unloading wave speeds, c_L and c_U, are given by

$$c_L = \sqrt{M_L/\rho}, \tag{10}$$

$$c_U = \sqrt{M_U/\rho}, \tag{11}$$

where M_L and M_U are the constrained moduli in loading and unloading and ρ is the mass density. For the unloading (elastic) case, the constrained modulus is given by the well-known expression

$$M_U = \frac{E(1-\nu)}{(1+\nu)(1-2\nu)}, \tag{12}$$

where E is Young's modulus and ν is Poisson's ratio.

To derive an equivalent expression for M_L, consider a uniaxial strain increment de_1 in the plastic loading (i.e., tensile) direction, with all other incremental strain components being zero. The volume strain increment $d\epsilon_{ii}$ is then given by $d\epsilon_{ii} = d\epsilon_{ii}^e + d\epsilon_{ii}^p = d\epsilon_1$. However, for the Prandtl–Reuss flow rule ($\alpha_p = 0$), the plastic volume strain increment $d\epsilon_{ii}^p$ is zero. Accordingly, the constitutive relation governing the elastic volume change can be written as

$$d\epsilon_1 = \frac{1-2\nu}{E}(d\sigma_1 + 2d\sigma_2), \tag{13}$$

which has used the fact that $d\sigma_2 = d\sigma_3$.

An additional constraint is provided by the fact that, during plastic flow, the stress state remains on the yield surface. As illustrated in Figure 2, this implies a linear relationship between the axial and lateral normal stress increments, $d\sigma_1$ and $d\sigma_2$. Using (1), this relationship is given by

$$d\sigma_1 = \frac{1-\sqrt{3}\alpha}{1+2\sqrt{3}\alpha}d\sigma_2, \tag{14}$$

where we have again exploited the fact that $d\sigma_2 = d\sigma_3$. Substituting (14) into (13) then leads to an incremental relationship of the form

$$d\sigma_1 = M_L d\epsilon_1, \tag{15}$$

where

$$M_L = \frac{E}{3(1-2\nu)}(1+2\sqrt{3}\alpha), \tag{16}$$

which is the desired expression for the loading modulus. Using a finite-element code that supports this simple nonassociated model, single-element uniaxial-strain testing of a closed strain path from the prestressed state will easily confirm both of these formulas for the loading and unloading moduli (as well as negative net work for a closed strain path). Such verification testing is an essential prerequisite before attempting to solve the more complicated wave-propagation problem (cf. Kamojjala et al. 2015).

The loading and unloading moduli and wave speeds for the example problem with the Prandtl–Reuss flow rule can be computed using (10), (11), (12) and (16), together with the previously specified material

properties. The values that are obtained are

$$M_L = 41.8 \, \text{GPa}, \quad c_L = 4.09 \, \text{km/s},$$
$$M_U = 36.0 \, \text{GPa}, \quad c_U = 3.79 \, \text{km/s}.$$

As seen, the loading modulus is sixteen percent greater than the unloading modulus, and the loading wave speed is eight percent greater than the unloading wave speed. Although the difference in the wave speeds may seem small, it will be shown in the next section that if there is *any* degree of achronicity at all, no matter how small, it can lead to arbitrarily large instabilities for this case study.

From (12) and (16), it is seen that $M_L > M_U$ if and only if

$$\alpha > \frac{1 - 2\nu}{\sqrt{3}(1+\nu)}. \tag{17}$$

For $\nu = 0.25$, this corresponds to $\phi > 30°$. Accordingly, for friction angles below this value, achronicity does not occur for longitudinal plane wave propagation with this particular flow rule. It can be shown that achronicity itself does still occur for many other modes of plane wave propagation, but the deformation modes that are involved are much more complex and multidimensional. The main reason for choosing a relatively high friction angle (40 degrees) for the example problem was to allow some of the features of achronicity to be illustrated with a deformation mode that is as simple as possible (uniaxial strain in both loading and unloading).

4. Analytical solutions

In this section, we show that the example problem can be solved analytically, resulting in infinitely many possible solutions. This is done by first deriving a family of solutions having two independent free parameters. The nonunique and unstable nature of these solutions is then illustrated by considering some example solutions chosen from this family.

One of the consequences of nonuniqueness is that there are many possible *families* of solutions having different functional forms. In the following discussion, we focus on only one such family, with a specific assumed functional form. Accordingly, the example solutions that are presented are not necessarily representative of all possible solutions, but merely sufficient to demonstrate nonuniqueness. However, as will later be seen, the features of these solutions are very similar to those of the numerical verification simulations in Section 5.

4.1. *Derivation.* The approach is similar to the one employed by Sandler and Rubin [1987]. We begin by first dividing the (x, t) plane into six regions, as illustrated in Figure 3. The boundaries of these regions are characteristics, along which the stress is constant in time. With perfect plasticity or linear hardening, all of the characteristics form straight lines in the (x, t) plane whose slope is equal to the wave speed. With nonlinear hardening the characteristics for plastic loading are no longer straight lines since the wave speed is no longer constant. The case of nonconstant plastic wave speed will be discussed in Section 5.

In each region, the material is assumed to be undergoing either plastic loading or elastic unloading, as indicated in the figure. (Note that region 1, which is the quiescent region ahead of the pulse, could be taken as either loading or unloading; for definiteness, we label it to be loading.)
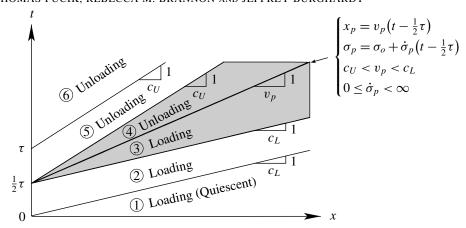
Figure 3. Regions in the (x, t) plane employed in constructing an analytical solution. The difference between the loading and unloading wave speeds is exaggerated for clarity. The shaded region is where the solution is nonunique.

Within each region, i, the equations of motion in the x-direction can then be expressed as

$$\rho \frac{\partial v}{\partial t} = \frac{\partial \sigma}{\partial x}, \tag{18}$$

$$\frac{\partial \sigma}{\partial t} = \rho c_i^2 \frac{\partial v}{\partial x}, \tag{19}$$

$$c_i = \begin{cases} c_L & \text{if } i = 1, 2, 3, \\ c_U & \text{if } i = 4, 5, 6, \end{cases} \tag{20}$$

where $\sigma(x, t)$ and $v(x, t)$ represent the changes in axial stress and velocity in the x-direction due to the perturbation, and are defined by

$$\sigma(x, t) = \sigma_{xx}(x, t) - \sigma_x^*, \tag{21}$$

$$v(x, t) = v_x(x, t). \tag{22}$$

As illustrated in the figure, region 2 represents the portion of the (x, t) plane swept out by the loading ramp propagating at the loading wave speed, c_L. Similarly, region 5 represents the portion swept out by the unloading ramp propagating at the unloading wave speed, c_U. Because $c_L > c_U$, the loading ramp travels faster than the unloading ramp, which causes the two ramps to separate. As noted earlier, this has two important consequences. The first is that the pulse width increases linearly with time. (The reason for this is readily apparent from the figure.) The second is that the region between these two ramps, which initially consists of a single point, opens up into a finite region (the region indicated by the shaded area). The solution in this region is indeterminate in that it is not dictated by either the initial conditions or the boundary conditions, as is normally the case for well-posed initial/boundary value problems for hyperbolic equations. As a result, it is unstable and nonunique. Another useful way of thinking about the origin of the nonuniqueness in this region is that there is no characteristic information in this region, making the wave speed indeterminate. A nearly identical phenomenon is well known to occur for other hyperbolic equations such as a rarefaction Riemann problem with the inviscid Burger's equation. In that

case and ours, there are multiple ways to construct characteristics for the region in question, resulting in multiple solutions. For details, see [LeVeque 1992, p. 28] and [Thomas 1999, p. 82].

Here we demonstrate one method of filling in the missing characteristic information in the shaded region of Figure 3. To do this we have divided the separated (shaded) region into two regions shown in the figure. In region 3, the material is assumed to undergo continued loading, while in region 4 it is assumed to be unloading. Accordingly, the boundary between the two regions represents the path followed by the peak axial stress perturbation in the (x, t) plane. The position and value of the peak axial stress perturbation are assumed to be given by

$$x_p(t) = v_p\left(t - \tfrac{1}{2}\tau\right), \tag{23}$$

$$\sigma_p(t) = \sigma_o + \dot{\sigma}_p\left(t - \tfrac{1}{2}\tau\right), \tag{24}$$

where $t \geq \tfrac{1}{2}\tau$, and where v_p and σ_p represent the propagation velocity and time rate of change of the peak axial stress perturbation, respectively. The latter two quantities are both assumed to be constant, and are treated as free parameters, subject only to the following restrictions:

$$c_U < v_p < c_L, \tag{25}$$

$$0 \leq \dot{\sigma}_p < \infty. \tag{26}$$

Note that the first inequality implies that the dashed line must lie somewhere inside the shaded region, but the precise location within this region is arbitrary. The second inequality ensures that the axial stress perturbation along this line, σ_p, does not decrease with time; however, the rate of increase, $\dot{\sigma}_p$, may have an arbitrarily large positive value.

The preceding assumptions would normally be considered improper for well-posed initial/boundary value problems. For well-posed problems, the solution is uniquely determined by the field equations, initial conditions, and boundary conditions. Prescribing values for the solution along an arbitrary line in the (x, t) plane represents an over-specification, which usually results in the problem having no solution (except, of course, for the special case where the values that are prescribed happen to agree with the solution that would have been obtained anyway). However, because the solution to the example problem is nonunique, it will be seen that it is always possible to obtain a solution for this "over-specified" problem for any values of the free parameters, v_p and $\dot{\sigma}_p$, in the ranges given in the inequalities (25) and (26).

To demonstrate this, we begin by assuming that the solution in each region, i, can be expressed in the functional form

$$\sigma(x, t) = \sigma^{(i)}(x, t) = A_i x + B_i\left(t - \tfrac{1}{2}\tau\right) + D_i, \tag{27}$$

$$v(x, t) = v^{(i)}(x, t) = \frac{B_i}{\rho c_i^2}x + \frac{A_i}{\rho}\left(t - \tfrac{1}{2}\tau\right) + \frac{E_i}{\rho}, \tag{28}$$

where A_i, B_i, D_i and E_i are constants that are yet to be determined. Since these expressions are linear in x and t, the solution surfaces for σ and v, which can be visualized in the third dimension above the (x, t) plane, are composed of planar surfaces above each region. These surfaces are assumed to join continuously along the boundaries between the regions, but the partial derivatives may be (and typically are) discontinuous at the boundaries.

It is easily verified that the functional forms assumed in (27) and (28) automatically satisfy the field equations given in (18) and (19) within each region, i, for any values of the unknown coefficients A_i, B_i, D_i and E_i. Accordingly, the values of these coefficients are dictated by the various conditions that are specified, which can be summarized as follows:

Initial conditions:

$$\sigma(x, 0) = v(x, 0) = 0 \quad \text{for } 0 \le x < \infty. \tag{29}$$

Boundary conditions:

$$\sigma(0, t) = \begin{cases} (2\sigma_o/\tau)t, & 0 \le t \le \frac{1}{2}\tau, \\ (2\sigma_o/\tau)(\tau - t), & \frac{1}{2}\tau \le t \le \tau, \\ 0, & \tau \le t \le \infty. \end{cases} \tag{30}$$

Peak axial stress condition:

$$\sigma(x, t) = \sigma_o + \dot{\sigma}_p\left(t - \tfrac{1}{2}\tau\right) \quad \text{on } x = v_p\left(t - \tfrac{1}{2}\tau\right),\ \tfrac{1}{2}\tau \le t < \infty. \tag{31}$$

Continuity conditions:

$$\left.\begin{aligned} \sigma^{(i+1)}(x, t) &= \sigma^{(i)}(x, t) \\ v^{(i+1)}(x, t) &= v^{(i)}(x, t) \end{aligned}\right\} \quad \text{on } x = v_b^{(i)}(t - t_b^{(i)}),\ t_b^{(i)} \le t < \infty,\ i = 1, \ldots, 5. \tag{32}$$

Loading conditions:

$$\frac{\partial \sigma}{\partial t} \ge 0 \quad \text{for } i = 1, 2, 3, \qquad \frac{\partial \sigma}{\partial t} \le 0 \quad \text{for } i = 4, 5, 6. \tag{33}$$

Consistent with (21), σ and v represent the changes in axial stress and velocity in the x-direction due to the applied perturbation. In (32), the quantity $v_b^{(i)}$ represents the propagation velocity of the boundary between regions i and $i + 1$, and $t_b^{(i)}$ represents its intercept on the t-axis, as illustrated in Figure 3. Also, the conditions given in the inequalities (33) ensure consistency with the assumption that the material is undergoing plastic loading in regions 1–3 and elastic unloading in regions 4–6.

Obtaining a solution to the above equations is straightforward but tedious, and a detailed derivation will not be given here. Instead, we simply state the solution, which is given by the set of coefficients shown in Table 1. It can be verified that these coefficients, the axial stress σ, and velocity v, defined in equations (27)–(28) satisfy (29)–(33) for any values of the free parameters v_p and $\dot{\sigma}_p$ in the ranges given by the inequalities (25)–(26). The existence of free parameters (having values not determined from the problem data) demonstrates that the governing equations have no unique solution. Following a few general observations about these solutions, the next subsection provides some representative examples illustrating the nonuniqueness and unstable nature of the solution.

As noted earlier, σ and v are continuous along the boundaries between regions, but their derivatives might be (and typically are) discontinuous. This so-called "weak" discontinuity does *not* violate any physical or mathematical law. In fact, similar propagating weak discontinuities would occur for a purely elastic material subjected to the same initial and boundary conditions. The equations of motion are satisfied in integral form across any control volume containing only weak discontinuities in stress and velocity (i.e., where σ and v themselves are both continuous; cf. Chapter 2 of [Drumheller 1998]).

i	c_i	A_i	B_i	D_i	E_i
1	c_L	0	0	0	0
2	c_L	$-\dfrac{2\sigma_o}{c_L \tau}$	$\dfrac{2\sigma_o}{\tau}$	σ_o	$-\dfrac{\sigma_o}{c_L}$
3	c_L	$-\dfrac{\dot{\sigma}_p}{c_L - v_p}$	$\dfrac{c_L \dot{\sigma}_p}{c_L - v_p}$	σ_o	$-\dfrac{\sigma_o}{c_L}$
4	c_U	$\dfrac{(c_L v_p + c_U^2)\dot{\sigma}_p}{c_L(v_p^2 - c_U^2)}$	$-\dfrac{c_U^2(c_L + v_p)\dot{\sigma}_p}{c_L(v_p^2 - c_U^2)}$	σ_o	$-\dfrac{\sigma_o}{c_L}$
5	c_U	$\dfrac{2\sigma_o}{c_U \tau} + \dfrac{(c_L - c_U)\dot{\sigma}_p}{cL(v_p + c_U)}$	$-\dfrac{2\sigma_o}{\tau}$	σ_o	$-\dfrac{\sigma_o}{c_L}$
6	c_U	$\dfrac{(c_L - c_U)\dot{\sigma}_p}{c_L(v_p + c_U)}$	0	0	$\dfrac{(c_L - c_U)\sigma_o}{c_L c_U}$

Table 1. Coefficients in the analytical solution.

One interesting difference between this case and the elastic case is that, in the elastic case (governed by the simple wave equation), discontinuities in derivatives can propagate only along characteristic lines in the (x, t) plane, the slope of which is uniquely determined from material properties. However, in the above solution, the discontinuity at the location of the peak stress propagates along a line that does *not* correspond to a characteristic of either the loading properties or unloading properties, but is somewhere in between. Such behavior is impossible with the simple wave equation, and may seem suspicious at first glance. The reason that it is possible here is that the material properties at any point on this line are undefined (or, more precisely, they are double-valued, and depend on which region one approaches the point from). A similar observation applies for ordinary associative elastic-plastic materials, but with the crucial difference that associativity of the flow rule ensures uniqueness of the velocity of the peak stress point, v_p. Such uniqueness is not the case for nonassociated flow rules.

It is also possible to derive an analytical solution for the case in which the perturbation applied to the surface of the region consists of a triangular *velocity* pulse rather than a triangular axial stress pulse. The form and features of this solution are very similar to those of the example problem discussed here, with one notable difference. With an axial stress pulse, the external forces may continue to do work on the region after the pulse is completed if the front surface has a nonzero velocity (which it generally does). However, with a velocity pulse, the external forces do no work after the pulse is completed, and the ambient forces (those associated with the prestress σ_{ij}^*) do no net work during the pulse. Accordingly, for purposes of illustrating the overall energy balance, a velocity pulse is actually more desirable than a stress pulse. The main reason for choosing a stress pulse for the example problem is that it provides a better illustration of some of the unusual characteristics of the nonassociated material response.

4.2. *Example solutions.* Example solutions corresponding to three different choices of the free parameters v_p and $\dot{\sigma}_p$ are illustrated in Figures 4, 5, and 6. The value of v_p is the same in all three cases (3.98 km/s), while $\dot{\sigma}_p$ ranges over three different values (0, 0.15, and 0.25 MPa/ms). For each case, the
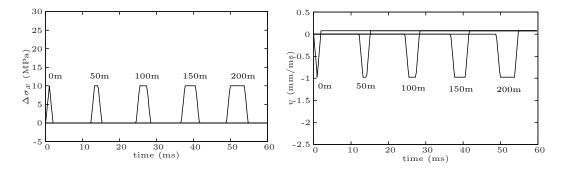
Figure 4. Time histories of axial stress and velocity with the free parameter $\dot{\sigma}_p = 0.0\,\text{MPa/ms}$, with the free parameter v_p equal to 3.98 km/s. The width of the wave is increasing linearly in time.
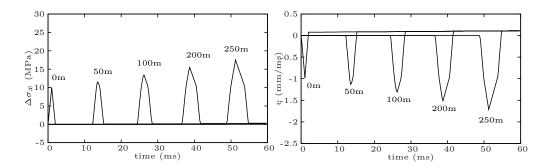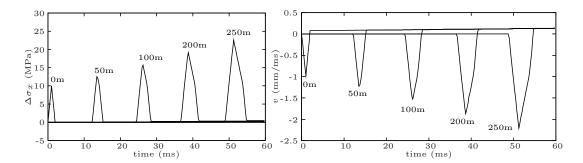

Figure 5. Time histories of axial stress and velocity with the free parameter $\dot{\sigma}_p = 0.15\,\text{MPa/ms}$, with the free parameter v_p equal to 3.98 km/s. This solution exhibits an increase in both the width and amplitude of the wave.

figure shows time histories of axial stress and velocity at various axial locations. The unstable nature of these solutions is readily apparent in that both the widths and the amplitudes of the pulses increase linearly with time (except for the special case where $\dot{\sigma}_p = 0$, where the amplitude remains constant). Nonuniqueness is thus demonstrated by fact that these three different results each represent solutions to the original initial/boundary value problem. Later, numerical results will be shown to corroborate this purely analytical conclusion.

The case $\dot{\sigma}_p = 0$ can be viewed as a baseline solution in which the pulse widens with time but does not grow in amplitude. The widening results from the fact that the loading ramp is traveling faster than the unloading ramp. Since $\dot{\sigma}_p = 0$, the solution is constant in the separated region between the two ramps. Accordingly, the initially triangular pulse evolves into a trapezoidal pulse that grows wider with time, at a rate proportional to $c_L - c_U$. The other two cases illustrate the effect of progressively increasing the peak stress growth rate $\dot{\sigma}_p$. The linear growth in peak stress with time (and also with distance) is evident in the figure. The main effect of this growth is to superimpose a triangular pulse on top of the flat top of the baseline solution. The base of this triangle grows with time at a rate proportional to $c_L - c_U$, while the height grows at a rate proportional to $\dot{\sigma}_p$.

Figure 6. Time histories of axial stress and velocity with the free parameter $\dot{\sigma}_p = 0.250$ MPa/ms. This solution exhibits an increase in both the width and amplitude of the wave. The rate of increase of the magnitude of the wave may be specified to be arbitrarily large.

Since the rate at which the pulse widens is proportional to $c_L - c_U$, it follows that reducing the degree of achronicity (i.e., reducing the difference between c_L and c_U) would likewise reduce widening of the pulse. However, the growth in the *amplitudes* of the pulses would be unaffected, since they are proportional to the independent free parameter $\dot{\sigma}_p$. In fact, since $\dot{\sigma}_p$ may have an arbitrarily large value, it follows that any degree of achronicity, no matter how small, still admits an instability that is arbitrarily large in magnitude.

After the main pulse has passed over a given material particle, the particle is left with a residual velocity. This can be seen in the velocity plots in Figures 4, 5, and 6. This is a common occurrence in inelastic wave propagation problems, and may not seem surprising at first glance. However, upon closer inspection, it is found that this velocity is in the *opposite direction* from what would normally be expected (i.e., in the negative x-direction, whereas the particle velocity for the main wave is in the positive x-direction).

The unstable nature of these solutions is further illustrated in Figure 7, which shows the total kinetic energy (per unit cross-sectional area) vs. time for the three example solutions shown in Figure 4. The kinetic energy generated while the surface perturbation is being applied (from 0 to 2 ms) is roughly 3.4 kJ/m^2, which is comparable to the energy that would be generated if the material response were purely elastic (about 3.5 kJ/m^2). However, in the elastic case, the kinetic energy would remain constant after the perturbation is over. For the elastic-plastic solution shown here, kinetic energy continues to increase. In contrast, the kinetic energy for an associated flow rule would decrease in time. For the special case $\dot{\sigma}_p = 0$, the kinetic energy is linear with time, which is consistent with the fact that the pulse width grows at a constant rate, but the amplitude remains constant. For the other two solutions, the amplitude also increases at a constant rate, which introduces quadratic and cubic terms.

A simple way of understanding the growth in kinetic energy is to consider what happens to an individual particle (i.e., an infinitesimal element of material). As noted earlier, for a regular nonassociated flow rule, it is always possible to find closed strain cycles for which the work done on a material particle is negative, i.e., the particle does work on its surroundings. This occurs for any strain cycle that corresponds to a trial elastic stress increment lying in the wedge-shaped region shown in Figure 2. In these solutions, as the propagating pulse passes over each material particle, it puts the particle through a loading cycle that

is close to (although not precisely) a closed strain cycle, with a trial elastic stress increment that is in the wedge. As a result, the particle does work on its surroundings, thus liberating some stored elastic energy, much of which shows up in the form of kinetic energy. Kinetic energy in these solutions can increase without bound even if the boundary stimulus is infinitesimal. Even though this behavior technically corresponds to spontaneous motion from a quiescent state, it does *not* violate thermodynamics, since energy is not being created; prestored strain energy is merely being released in an unstable manner. As this process continues, the total kinetic energy continues to increase as long as there is material in an achronic state for the pulse to propagate into. Of course, for real specimens of finite dimension, an infinite kinetic energy would never be realized. As discussed later, observable characteristics of this instability (if real) in finite samples remains are unclear, but its potential existence merits much expanded laboratory investigation as well as first-principles theories to provide a microphysical basis for the behavior (if real). Novel experimental methods are needed to determine if the phenomenon of unstable liberation of elastic stored energy is physically possible, or merely an anomalous artifact of insufficient sophistication of classical nonassociated regular plastic flow rules.

Although most of the growth in kinetic energy comes from the release of prestored strain energy, there is a relatively small contribution from work done by traction acting on the surface of the half-space. From Figure 4, it can be seen that there is a small positive residual velocity at the surface after the perturbation has been completed. Since the ambient stresses from the prestress are compressive, this means that they continue to do positive work on the region. These instabilities are not somehow being fueled by this ever-increasing boundary work after the axial stress pulse has been applied. In fact, the continual rise in kinetic energy is entirely consistent with (a violation of) Drucker's stability postulates, which state that, for a stable plastic material, useful energy cannot be extracted from a material *and the system of forces acting on it* over a closed loading cycle [Drucker 1949; 1950]. Moreover, as mentioned earlier, analytical solutions can also be derived for problems in which the perturbation applied at the surface is a triangular velocity pulse rather than a triangular axial stress pulse, in which case the results are very similar to the results shown here even though *the post-pulse boundary loads do no work whatsoever*. The main difference is that the residual stress and velocity behind the main pulse are slightly different, and the kinetic energy vs. time curves are reduced by about 10 percent.[5]

5. Numerical solutions

An interesting question is whether the instabilities exhibited by these analytical solutions actually occur in numerical simulations. There are some legitimate reasons to think they might not. For example, since they emanate from a single point in space and time, they must always pass through a phase where they are too small to be resolved (spatially and/or temporally) in most numerical schemes. Also, most numerical simulations incorporate some form of viscosity (real and/or artificial), which introduces higher-order terms into the equations that Sandler and Rubin [1987] conjectured might cause the solutions to become unique. Of course, even if it turned out that instability and nonuniqueness *were* ruled out for these (or any

---

[5] Although the boundary tractions have little effect on the kinetic energy, the amount of work they do is nontrivial. For the three solutions shown in Figure 4, boundary work is of the order of 500 kJ/m^2 at $t = 60$ ms. However, when compared to the corresponding solutions for velocity perturbations, it is found that almost all of this work ends up as residual strain energy rather than as kinetic energy. To put this in perspective, a change in the residual strain energy of this magnitude corresponds to a change in residual stress of less than 1 MPa.
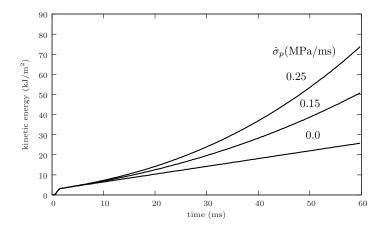
Figure 7. Total kinetic energy per unit cross-sectional area (i.e., $\int_0^\infty \frac{1}{2}\rho v \cdot v\, dx$) for the three analytical solutions shown in Figures 4, 5, and 6.

other) reasons, it would not justify the answers one gets using these simulations if the reasons were purely numerical, or lacked a physical basis. Nevertheless, it does raise some interesting numerical issues.

Even if instabilities do occur, it is not clear what form they might take. The family of solutions considered in the preceding section is only one of many possible families, and is itself doubly infinite (i.e., there are two free parameters, each of which may take on an infinite number of values). Yet, a digital computer will always give one and only one answer. Moreover, since the arithmetic operations it performs are completely deterministic, it will always give *exactly* the same answer no matter how many times you rerun the calculation, as long as the inputs (and computing hardware) are *exactly* the same. This raises some obvious questions: Which instability (if any) does the computer select? How does nonuniqueness manifest itself in numerical simulations?

To explore these questions, some numerical simulations were carried out using several finite-element codes (DYNA3D, ABAQUS, and a one-dimensional code of our own writing), as well as the explicit material point method (MPM) code Uintah. The results from the analysis using all of these codes were similar, but, as would be expected from the lack of unique solution to this problem, the numerical solutions differed slightly from code to code. The numerical solutions shown here are all those from the Uintah MPM code. For a comprehensive discussion of the MPM, and the similarities and differences between it and the finite-element method, the reader is referred to Sadeghirad et al. [2011]. A detailed description of how the problem was set up for the MPM will be given here, along with some comments on how the problem was solved with the various finite-element codes.

For the Uintah simulations the problem domain was discretized into a 700 meter long line of 3D rectangular cells with two MPM particles per cell. For the two commercial codes a single line of hex-ahedral elements was used. Although the strain increments associated with the perturbation involve pure uniaxial strain, the initial state σ^* is not a uniaxial strain state. Two approaches have been used to attain the initial conditions for this problem. The ABAQUS simulations began at a unstressed state with the loads gradually being increased to the desired stress state. After the desired conditions were reached, further lateral displacement was constrained and the axial stress perturbation was applied. In the DYNA3D and Uintah simulations, the constitutive model was modified so that stresses and strains
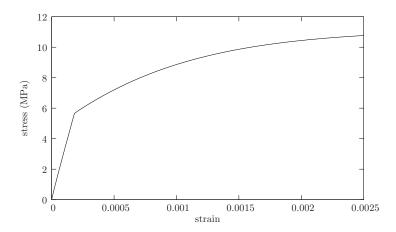
Figure 8. Uniaxial stress versus strain plot for the nonlinear hardening model used for numerical solutions.

would be measured relative to the prestressed state, rather than the unstressed state. This eliminated the need for the initialization phase, and the lateral (y- and z-faces) boundaries are constrained to have zero lateral displacement throughout the simulation. In accordance with the problem description given in Section 2, one x-face of the domain had an applied traction boundary condition given by (4)–(7), and the opposite x-face of the domain is specified to have zero displacement in the x-direction.

The case-study problem was solved using both the perfect-plasticity constitutive model used for the analytical solutions derived in Section 4 as well as a similar linear Drucker–Prager model with the nonlinear hardening yield function

$$f = \sqrt{J_2} + \alpha I_1 - k_{\text{limit}} - (k_o - k_{\text{limit}})e^{-z/z_{\text{ref}}}, \tag{34}$$

where k_{limit} is the maximum value of the yield strength, z is the cumulative equivalent plastic strain, and z_{ref} is a parameter that controls the rate at which the maximum yield strength is approached.

The nonlinear hardening parameters were chosen to be $k_{\text{limit}} = 10\,\text{MPa}$ and $z_{\text{ref}} = 0.001$. Figure 8 shows axial stress versus axial strain for a uniaxial stress loading path with the nonlinear hardening model with the chosen parameter values. As the plot clearly indicates, the plastic tangent modulus (and thus the plastic wave speed) is continually changing with plastic loading.

5.1. *Temporal and spatial convergence.* An initial element length of 0.5 m was chosen for use in a temporal convergence study. The Courant–Friedrichs–Lewy (CFL) time step was calculated from the elastic properties as is commonly done in explicit finite-element codes. It was discovered that the solution became unstable for time steps greater than 0.8 times the CFL time step calculated from the elastic properties. This was to be expected since the plastic wave speed is greater than the elastic wave speed for this problem. Figure 9 is a plot of the peak change in axial stress caused by the propagating wave at a point 600 meters into the problem domain for various time step factors. The time step factor is defined as the ratio of the actual time step used in a simulation to the CFL time step calculated from the elastic wave speed. As the figure shows, the numerical simulation converged with respect to the time step size with a time step of approximately 10% of the CFL time step.
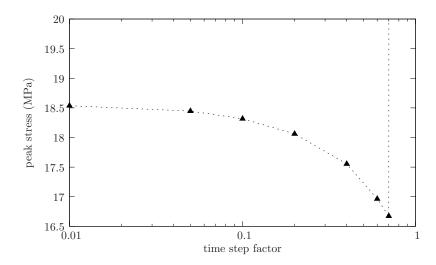
Figure 9. Plot of the change in axial stress caused by the stress wave at a location 600 meters into the problem domain for various time step factors. The time step factor is the ratio of the actual time step used int he simulation to the CFL time step calculated from the elastic properties of the material. The peak axial stress appears to have converged at approximately 10% of the elastic CFL time step.

In accordance with the temporal convergence study, several simulations were performed with the time step set to 10% of the CFL time step and a progressively smaller element length. Figure 10 shows some numerical solutions of the example problem. As the plots show, the solutions with a mesh resolution of 0.5 m and 0.25 m appear very similar, giving the impression that the solution has converged. However, if the mesh spacing is reduced again, the solution changes considerably, with secondary peaks forming approximately 500 meters into the domain. These secondary peaks grow at a more rapid rate than the primary peak. If the mesh is refined further these secondary peaks form earlier and earlier, and grow at an increased rate without bound. While we have only shown solutions from the Uintah MPM code, the results from the ABAQUS and DYNA3D exhibited the same trends with mesh refinement.

For the simulations performed in DYNA3D, it was found that two simulations with identical input parameters but with a different number of time history output blocks produced dramatically different solutions. It was found that the preprocessor had altered the seventh or eighth digit of the initial locations of approximately 10% of the nodes. It appears that the numerical solution is very sensitive to small changes in the initial conditions of the simulation. This chaos appears to be a manifestation of the nonuniqueness discussed in Section 4.

Stoughton and Yoon [2008] have asserted that the Sandler–Rubin instability cannot exist if the plastic tangent modulus is not constant to first order. The basis for this assertion is that, if nonconstant wave speeds are substituted into the Sandler–Rubin solution, the resulting expressions fail to satisfy the governing equations. However, as discussed above, this does not mean that the Sandler–Rubin instability cannot exist if the wave speed is not constant — it simply means that the Sandler–Rubin analytical solution was limited to the special case of a constant wave speed. Accordingly, there is no reason to expect that such a solution should apply to a nonconstant wave speed.
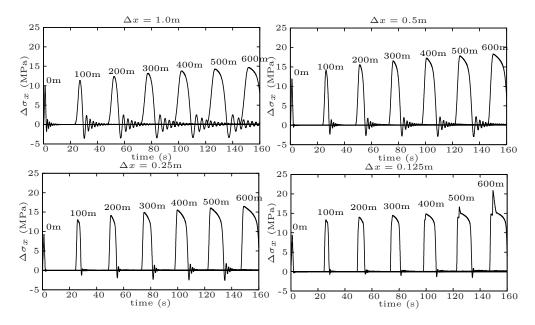
Figure 10. Numerical solutions to the case study problem with perfect plasticity and 1 m, 0.5 m, 0.25 m, and 0.125 m cell widths, illustrating the lack of convergence with mesh refinement. As the axial stress histories with $\Delta x = 0.125$ m indicate, as the mesh is refined additional peaks in the waveform appear that grow rapidly in time. These additional peaks form at earlier and earlier times as the mesh is refined further.

Stoughton defines several classes of plasticity models that do not result in a constant plastic tangent modulus, and therefore were claimed not to admit the Sandler–Rubin instability. One class of models that has this attribute is any model with nonlinear hardening. Although somewhat counterintuitive, it is shown in the companion paper that, for achronic loading conditions, hardening actually reduces the wave speed, and softening increases the wave speed, as compared to a perfectly plastic response. Therefore, hardening would be expected to reduce the degree of achronicity (i.e., the degree to which the plastic wave speed is faster than the elastic wave speed) when the material initially yields. However, with most nonlinear hardening functions, including the one chosen for this example, the tangent hardening modulus decreases as the material undergoes plastic deformation, which will cause the plastic wave speed to approach the perfect plasticity wave speed as plastic flow continues. For the purpose of the example problem considered here, in the x-t diagram for the nonlinear hardening case the characteristics for the head of the wave, which are undergoing plastic deformation, will still diverge from the characteristics for the tail of the wave, which is undergoing elastic deformation. The primary difference is that characteristics on the head of the wave will not be parallel, since at each point of the wave the material will have undergone a different amount of plastic deformation and will therefore have a different plastic tangent modulus and hence a different wave speed. However, for all points on the head of the wave, the wave speed will exceed the elastic wave speed, which will cause the development of the region between the head and tail of the wave to form, which has no uniquely defined characteristics and hence no unique solution.
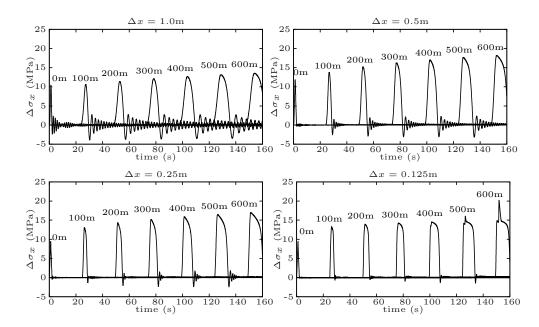
Figure 11. Numerical solutions to the case study problem with the nonlinear hardening model given in (34) and 1 m, 0.5 m, 0.25 m, and 0.125 m element lengths, illustrating the lack of convergence with mesh refinement even with the nonlinear hardening model for which the plastic wave speed is not constant. As with the nonhardening case, additional peaks in the waveform and an increase in instability develop with a mesh spacing of 0.125 m. Further mesh refinement results in these additional peaks occurring even earlier and growing more rapidly.

To illustrate that a nonlinear hardening model does admit the Sandler–Rubin instability, the same case study problem was solved with the nonlinear hardening Drucker–Prager model given in (34). The axial stress histories found using this model and mesh spacings of 1 m, 0.5 m, 0.25 m, and 0.125 m are shown in Figure 11. To assuage any lingering concerns that this instability is the result of time-integration instability, for these results we used a time step of one one-hundredth of the CFL time step calculated using the elastic stiffness, which is an order of magnitude smaller than the time step used to generate the plots in Figure 10. As the axial stress histories indicate, just as with the nonhardening case, the instability remains and the solution does not converge with mesh refinement, suggesting that the governing equations remain ill-posed for this case.

6. Conclusion

In this paper we have introduced a simple case study that illustrates an instability that has long been known to be caused by nonassociated plastic flow, but which has been largely overlooked in the literature in comparison to better-known instabilities such as localization or flutter. The mathematical origin of this instability is referred to as achronicity, in which the wave speed in plastic loading exceeds that in elastic unloading. A key goal of this work is to call attention to the lack of experimental evidence

validating or invalidating existence of achronicity, which is predicted for *any* nonassociated regular flow rule. It was shown that this condition can lead to both instability and nonuniqueness of solutions to the equations of motion. This assertion was demonstrated analytically by showing that the problem has a two-parameter family of nonunique solutions, which are unstable in that both the width, amplitude, and kinetic energy of the pulse all increase with time. It was then demonstrated that similar instabilities also occur in numerical calculations, where thorough attention was paid to ensuring that the instability was *not* caused by an insufficiently small time step. The nonuniqueness of nonassociative plasticity causes the numerical solutions to fail to converge with mesh refinement. The solutions are, in some cases, chaotically sensitive to small changes in the inputs. The mechanism that drives these instabilities is an unstable conversion of prestored strain energy into kinetic energy. The loading paths in this problem are similar in character to those discussed by Drucker [1949; 1950] and Il'Yushin [1961] in their discussions of stability of plasticity models more than fifty years ago, so the novel and worthwhile aspect of this work lies in the formulation of the illustrative case study itself. The case study demonstrates that this anomaly (which is not known to be real or merely a symptom of an insufficiently sophisticated model) still exists today in simple constitutive models commonly available in production finite-element codes, thus calling into question the mathematical well-posedness of any engineering application of such models.

The instabilities are very mild. Their growth rate is only linear with time, and only a small fraction of the prestored strain energy is actually converted into energy of motion. However, it is *precisely* these characteristics that cause them to be among the most insidious forms of instability. They can grow large enough to affect the answer, while staying small enough to not cause obvious problems such as code crashes from excessive deformation.

This achronic instability can be contrasted with other well-known forms of instability, such as time-stepping instabilities in explicit numerical calculations, which grow exponentially with time. Although time step instabilities are more serious in principle, they could be viewed as less serious in practice, precisely because they grow rapidly enough to quickly call attention to themselves. Achronic instabilities, on the other hand, are much less catastrophically disruptive, and much more difficult to detect in complex calculations. However, it is possible to detect achronicity by monitoring certain easily evaluated directional invariants of the elastic-plastic tangent stiffness tensor [Brannon and Drugan 1993].

A key purpose of this paper has been to reveal gaps in experimental data that prevent ascertaining if the Sandler–Rubin instability is real, or just a numerical and theoretical artifact of an ill-posed constitutive model. Part II of this paper explores the influence of various nonclassical constitutive model features on the instability, but the question of whether or not the instability is realistic remains open, pending careful experimental investigations of loading into the Sandler–Rubin wedge. Stoughton and Yoon [2008; 2012] conjectured what might serve as possible physical mechanisms and symptoms of the instability if it is indeed real (e.g., Lüders bands or serrated flow observed in some aluminum alloys at room temperature range). Again, these are conjectures for which systematic laboratory investigations of material response in the Sandler–Rubin wedge are warranted, but not yet achieved. Direct observations of material response (especially detection of negative net work in closed strain cycles) for loading into the Sandler–Rubin wedge would be a natural first focus area for laboratory testing. As discussed by Brannon et al. [2009], such experimental efforts are highly nontrivial because a statistically significant number of experiments must be conducted to identify the yield surface and apparent flow direction at a given stress state so that the location of the Sandler–Rubin wedge can be determined. For this reason,

exploratory *numerical* modeling of realistic microstructures (such as computed-tomography images of rock) might be appropriate because, unlike real laboratory testing, the material state can be *exactly* reset to probe path-dependent responses to various loading directions.

Acknowledgments

References

[Besse and Mohr 2012] C. C. Besse and D. Mohr, "Plasticity of formable all-metal sandwich sheets: Virtual experiments and constitutive modeling", *Int. J. Solids Struct.* **49**:19–20 (2012), 2863–2880.

[Bigoni 1995] D. Bigoni, "On flutter instability in elastoplastic constitutive models", *Int. J. Solids Struct.* **32**:21 (1995), 3167–3189.

[de Borst et al. 1993] R. de Borst, L. Sluys, H. Muhlhaus, and J. Pamin, "Fundamental issues in finite element analyses of localization of deformation", *Eng. Computation.* **10**:2 (1993), 99–121.

[Brannon 2007] R. M. Brannon, "Elements of phenomenological plasticity: Geometrical insight, computational algorithms, and topics in shock physics", pp. 225–274 in *ShockWave science and technology reference library*, edited by Y. Horie, Springer, Berlin, 2007.

[Brannon and Drugan 1993] R. M. Brannon and W. J. Drugan, "Influence of nonclassical elastic-plastic constitutive features on shock wave existence and spectral solutions", *J. Mech. Phys. Solids* **41**:2 (1993), 297–330.

[Brannon et al. 2009] R. Brannon, J. Burghardt, D. Bronowski, and S. Bauer, "Experimental assessment of unvalidated assumptions in classical plasticity theory", Report SAND2009-0351, Sandia National Laboratory, 2009, Available at http://www.mech.utah.edu/~brannon/pubs/7-BrannonBurghardtSAND-Report2009-0351.pdf.

[Cvitanic et al. 2008] V. Cvitanic, F. Vlak, and Z. Lozina, "A finite element formulation based on non-associated plasticity for sheet metal forming", *Int. J. Plast.* **24**:4 (2008), 646–687.

[Desmorat and Marull 2011] R. Desmorat and R. Marull, "Non-quadratic Kelvin modes based plasticity criteria for anisotropic materials", *Int. J. Plast.* **27**:3 (2011), 328–351.

[Drucker 1949] D. C. Drucker, "Relation of experiments to mathematical theories of plasticity", *J. Appl. Mech.* (*ASME*) **16** (1949), 349–357.

[Drucker 1950] D. C. Drucker, "Some implications of work hardening and ideal plasticity", *Quart. Appl. Math.* **7** (1950), 411–418.

[Drumheller 1998] D. S. Drumheller, *Introduction to wave propagation in nonlinear fluids and solids*, Cambridge Univ. Press, 1998.

[Dunand et al. 2012] M. Dunand, A. P. Maertens, M. Luo, and D. Mohr, "Experiments and modeling of anisotropic aluminum extrusions under multiaxial loading, I: Plasticity", *Int. J. Plast.* **36** (2012), 34–49.

[Gao et al. 2011] X. Gao, T. Zhang, J. Zhou, S. M. Graham, M. Hayden, and C. Roe, "On stress-state dependent plasticity modeling: Significance of the hydrostatic stress, the third invariant of stress deviator and the non-associated flow rule", *Int. J. Plast.* **27**:2 (2011), 217–231.

[Il'Yushin 1961] A. Il'Yushin, "On postulate of plasticity", *J. Appl. Math. Mech.* **25**:3 (1961), 746–752.

[Kamojjala et al. 2015] K. Kamojjala, R. Brannon, A. Sadeghirad, and J. Guilkey, "Verification tests in solid mechanics", *Eng. Comput.* **31**:2 (2015), 193–213.

[Lade et al. 1987] P. V. Lade, R. B. Nelson, and Y. M. Ito, "Nonassociated flow and stability of granular materials", *J. Eng. Mech. (ASCE)* **113**:9 (1987), 1302–1318.

[LeVeque 1992] R. J. LeVeque, *Numerical methods for conservation laws*, 2nd ed., Birkhäuser, Basel, 1992.

[Mohr et al. 2010] D. Mohr, M. Dunand, and K.-H. Kim, "Evaluation of associated and non-associated quadratic plasticity models for advanced high strength steel sheets under multi-axial loading", *Int. J. Plast.* **26**:7 (2010), 939–956.

[Rousselier et al. 2012] G. Rousselier, M. Luo, and D. Mohr, "Macroscopic plasticity modeling of anisotropic aluminum extrusions using a Reduced Texture Methodology", *Int. J. Plast.* **30–31** (2012), 144–165.

[Rudnicki and Rice 1975] J. Rudnicki and J. R. Rice, "Conditions for the localization of deformation in pressure-sensitive dilatant materials", *J. Mech. Phys. Solids* **23**:6 (1975), 371–394.

[Sadeghirad et al. 2011] A. Sadeghirad, R. M. Brannon, and J. Burghardt, "A convected particle domain interpolation technique to extend applicability of the material point method for problems involving massive deformations", *Int. J. Numer. Methods Eng.* **86**:12 (2011), 1435–1456.

[Sandler and Pučik 1993] I. S. Sandler and T. A. Pučik, "Non-uniqueness in dynamic rate-independent non-associated plasticity", Technical Report DNA-TR-92-108, Defense Nuclear Agency, 1993, Available at http://tinyurl.com/qg92z3k.

[Sandler and Rubin 1987] I. S. Sandler and D. Rubin, "The consequences of non-associated plasticity in dynamic problems", pp. 345–353 in *Constitutive laws for engineering materials* (Tucson, AZ), edited by C. Desai, Elsevier, Amsterdam, 1987.

[Shen et al. 2012] W. Shen, J. Shao, D. Kondo, and B. Gatmiri, "A micro-macro model for clayey rocks with a plastic compressible porous matrix", *Int. J. Plast.* **36** (2012), 64–85.

[Spitzig et al. 1975] W. A. Spitzig, R. J. Sober, and O. Richmond, "Pressure dependence of yielding and associated volume expansion in tempered martensite", *Acta Metall.* **23**:7 (1975), 885–893.

[Spitzig et al. 1976] W. A. Spitzig, R. J. Sober, and O. Richmond, "The effect of hydrostatic pressure on the deformation behavior of maraging and HY-80 steels and its implications for plasticity theory", *Metall. Trans. A* **7**:11 (1976), 1703–1710.

[Stoughton 2002] T. B. Stoughton, "A non-associated flow rule for sheet metal forming", *Int. J. Plast.* **18**:5–6 (2002), 687–714.

[Stoughton 2012] T. Stoughton, Informal communication, 2012. Email dated Jan. 13, 2012.

[Stoughton and Yoon 2008] T. Stoughton and J. W. Yoon, "On the existence of indeterminate solutions to the equations of motion under non-associated flow", *Int. J. Plast.* **24**:4 (2008), 583–613.

[Taherizadeh et al. 2010] A. Taherizadeh, D. E. Green, A. Ghaei, and J.-W. Yoon, "A non-associated constitutive model with mixed iso-kinematic hardening for finite element simulation of sheet metal forming", *Int. J. Plast.* **26**:2 (2010), 288–309.

[Thomas 1999] J. W. Thomas, *Numerical partial differential equations: Conservation laws and elliptic equations*, Texts in Applied Mathematics **33**, Springer, New York, 1999.

THOMAS PUČIK: *(Deceased) Pučik Consulting, 2057 Brixham Dr., Roseville, CA 95747, United States*

REBECCA M. BRANNON: rebecca.brannon@utah.edu
University of Utah, 50 S. Campus Dr., Salt Lake City, UT 84108, United States

JEFFREY BURGHARDT: jburghardt@slb.com
Schlumberger, 1935 S. Fremont Dr., Salt Lake City, UT 84104, United States

JOURNAL OF MECHANICS OF MATERIALS AND STRUCTURES

msp.org/jomms

Founded by Charles R. Steele and Marie-Louise Steele

Cover photo: Ev Shafrir